

See discussions, stats, and author profiles for this publication at: <https://www.researchgate.net/publication/339037441>

Fuel Injection Strategy for Utilization of Mineral Diesel–Methanol Blend in a Common Rail Direct Injection Engine

Article in *Journal of Energy Resources Technology, Transactions of the ASME* · February 2020

DOI: 10.1115/1.4046225

CITATIONS

26

READS

254

5 authors, including:



Akhilendra Pratap Singh

Indian Institute of Technology Kanpur

102 PUBLICATIONS 3,600 CITATIONS

[SEE PROFILE](#)



Nikhil Sharma

Indian Institute of Technology Kanpur

35 PUBLICATIONS 705 CITATIONS

[SEE PROFILE](#)



Vikram Kumar

Indian Institute of Technology Kanpur

46 PUBLICATIONS 748 CITATIONS

[SEE PROFILE](#)



Dev Prakash Satsangi

Indian Institute of Technology Kanpur

8 PUBLICATIONS 261 CITATIONS

[SEE PROFILE](#)

Akhilendra Pratap Singh

Engine Research Laboratory,
Department of Mechanical Engineering,
Indian Institute of Technology Kanpur,
Kanpur 208016, Uttar Pradesh, India

Nikhil Sharma

Engine Research Laboratory,
Department of Mechanical Engineering,
Indian Institute of Technology Kanpur,
Kanpur 208016, Uttar Pradesh, India

Vikram Kumar

Engine Research Laboratory,
Department of Mechanical Engineering,
Indian Institute of Technology Kanpur,
Kanpur 208016, Uttar Pradesh, India

Dev Prakash Satsangi

Engine Research Laboratory,
Department of Mechanical Engineering,
Indian Institute of Technology Kanpur,
Kanpur 208016, Uttar Pradesh, India

Avinash Kumar Agarwal¹

Engine Research Laboratory,
Department of Mechanical Engineering,
Indian Institute of Technology Kanpur,
Kanpur 208016, Uttar Pradesh, India
e-mail: akag@iitk.ac.in

Fuel Injection Strategy for Utilization of Mineral Diesel-Methanol Blend in a Common Rail Direct Injection Engine

Methanol fueled internal combustion (IC) engines have attracted significant attention due to their contributions in reducing environmental pollution and fossil fuel consumption. In this study, a single-cylinder research engine was operated on MD10 (10% (v/v) methanol blended with mineral diesel) and baseline mineral diesel to explore an optimized fuel injection strategy for efficient combustion and reduced emissions. The experiments were conducted at constant engine speed (1500 rpm) and load (3 kW) using two different fuel injection strategies, namely, single pilot injection (SPI) and double pilot injection (DPI) strategy. For each pilot fuel injection strategy, the start of main injection (SoMI) timing was varied from -3 to 6° crank angle (CA) before top dead center (bTDC). To examine the effect of fuel injection pressure (FIP), experiments were performed at three different FIPs (500, 750, and 1000 bars). Results showed that the MD10 fueled engine resulted in superior combustion compared with baseline mineral diesel, which was further improved by DPI at higher FIPs. The use of DPI strategy was found to be more effective at higher FIPs, resulting in higher brake thermal efficiency (BTE), lower exhaust gas temperature (EGT), and reduced oxides of nitrogen (NO_x) emissions compared with SPI strategy. Detailed investigations showed that the addition of methanol in mineral diesel reduced particulates, especially the accumulation mode particles (AMP). Different statistical analysis and qualitative correlations between fuel injection parameters showed that higher FIP and advanced SoMI timings were suitable for particulate reduction from the MD10 fueled engine. [DOI: 10.1115/1.4046225]

Keywords: methanol, common rail direct injection, fuel injection pressure, start of injection timing, particulates, alternative energy sources, energy conversion/systems, energy from biomass, fuel combustion, renewable energy, unconventional petroleum

1 Introduction

Excellent fuel economy, drivability, durability, and robustness make compression ignition (CI) engines more popular compared with spark ignition (SI) engines for various applications in transportation, agricultural, and industrial sectors. Due to the use of overall lean fuel-air mixtures and excellent fuel economy, CI engines emit relatively lower carbon monoxide (CO), hydrocarbons (HC), and carbon dioxide (CO_2) than their SI engine counterparts for the same power output. However, higher emissions of oxides of nitrogen (NO_x) and particulates remain a major concern for CI engines, which limit their applications in congested metro-cities globally [1,2]. On the other hand, most existing CI engines are operated using mineral diesel derived from depleting petroleum reserves. Recent studies showed that health issues from the exposure to pollutants from diesel engines (mainly NO_x and particulates) result in a very high cost to the society and human health due to short-term and long-term illnesses and premature deaths [1–5]. These environmental, health, and sustainability issues associated with mineral diesel fuelled combustion systems have motivated the researchers to explore viable renewable alternatives to mineral diesel. Continuous efforts to develop sustainable alternative fuels have yielded several options such as biodiesel, alcohols, dimethyl ether (DME), etc. From a

sustainability perspective, different aspects related to production, utilization strategies, and effects of these alternative fuels on the environment and human health have been critically examined by a large number of researchers [6–12]. Previous studies showed that alcohols produced from biomass using different biochemical processes have significant potential to be adapted as alternative fuels in the automotive sector. Alcohols produced from biomass are renewable and carbon-neutral fuels and their utilization in internal combustion (IC) engines leads to cleaner burning. Researchers have also investigated the uses of oxygenated additives such as alcohols [6–9,13–15] and biodiesels [9,10,14] on the CI engine performance and emissions. Presence of oxygenated additives in mineral diesel reduces particulate emissions [16–19]. Cheng et al. [20] suggested that the use of oxygenated additives also lowers the particulate- NO_x trade-off, which gives more flexibility for application of exhaust gas after-treatment systems. The presence of oxygen in test fuels enhances the premixed combustion phase and improves the diffusion combustion phase, thus lowering particulate formation due to oxygen-deficient conditions prevailing in the fuel-rich regions of the combustion chamber [21–23].

Although alcohols offer several advantages, however utilization of alcohols in CI engines has several challenges, which prevents its extensive utilization in production-grade CI engines. Alcohols and their blends with mineral diesel have several challenges including lower heating value (LHV), alcohol-mineral diesel immiscibility, as well as blends instability issues [24], lower cetane number (CN) of methanol, and poor lubricating properties [25]. There are few primary alcohols, which can be used as an additive in mineral diesel to enhance its fuel properties however each one

¹Corresponding author.

Contributed by the Internal Combustion Engine Division of ASME for publication in the JOURNAL OF ENERGY RESOURCES TECHNOLOGY. Manuscript received November 12, 2019; final manuscript received January 3, 2020; published online February 4, 2020. Assoc. Editor: Hameed Metghalchi.

has its own specific features. Solubility of alcohols in mineral diesel have been extensively studied by researchers and it is reported that lower blends of alcohol-mineral diesel blends reduce engine power output, which results in higher brake-specific fuel consumption (BSFC) [24,26–28]. Ethanol has been explored extensively for its feasibility in diesel engines because it can be produced from biomass; however, relatively lower energy density and strong hydrophilic nature are the main hurdles to be overcome for its utilization in a blended form with mineral diesel [29,30]. Researchers also investigated butanol because it is a good solvent for petroleum-based fuels and exhibits a much less hygroscopic behavior than ethanol [31,32]. However, relatively higher toxicity of butanol fueled engine exhaust and its incompatibility with fuel system components such as fuel filter (filter clogging), seal (softening and dissolution), etc., are some critical issues, which need to be addressed [31]. Methanol is the first member of the alcohol family, and it has gained significant attention from the researchers for automotive applications off-late.

Methanol is a low cost, non-sooting, and high oxygen content (~50% w/w) additive [33,34], which can be produced from various renewable resources. Relatively longer ignition delay of methanol due to low cetane number and high ignition temperature leads to smoother combustion of methanol-mineral diesel (MD) blends compared with baseline mineral diesel. High oxygen content and high H/C ratio of MD blends results in a relatively lower air-fuel stoichiometric ratio, which improves the combustion and reduces emission of particulates. Higher heat of vaporization and lower heating value of methanol results in lower flame temperature during combustion, leading to lower NO_x emissions but slightly higher HC and CO emissions [33,35]. Guo et al. [36] reported relatively higher BSFC for MD blends due to lower heating value of methanol; however, brake-specific energy consumption (BSEC) of MD blends was lower compared with mineral diesel. Shore et al. [37] suggested that lower molecular weight and simpler structure of methanol compared with mineral diesel also reduced particulate formation during the combustion of MD blends. MD blends also showed different spray characteristics and diluted the lubricant film on the piston wall, which adversely affected engine durability [38]. Therefore, fuel injection strategy including start of injection (SoI) timing, fuel injection pressure (FIP), and the number of injections becomes important for MD blends. Similar to mineral diesel-fueled engines, increasing FIP improved the combustion and emission characteristics of MD blends [39,40]. Sayin et al. [41] reported that deviation of SoI timing from its optimized range affected engine performance and emission characteristics. They reported that retarding the SoI timing resulted in higher HC emissions and advancing SoI timing led to higher NO_x emissions.

Previous studies showed that the complete replacement of mineral diesel with methanol is very challenging. Therefore, this research effort is focused on partial replacement of mineral diesel by methanol and adding a co-solvent to MD blends, which helps avoid phase separation. In this study, the experiments were conducted by adding 1% (v/v) 1-dodecanol as a co-solvent in MD10 (10% (v/v) methanol blended with mineral diesel) as recommended by Murayama et al. [42]. Fuel composition was chosen based on the results of previous investigations, where 10% blending of methanol with mineral diesel was found to be optimum for IC engine applications [43]. To investigate the effects of fuel injection parameters on engine combustion, performance, and emission characteristics, experiments were performed using different fuel injection strategies. To resolve the issue of fuel-air mixing, two different pilot injection strategies, namely, single pilot injection (SPI) and double pilot injection (DPI) were also evaluated. Detailed characterisation of the particulates emitted by the engine operated at different fuel injection strategies is the innovative aspect of this study. Qualitative correlations of emissions and performance parameters with particulates characteristics show some interesting aspects of utilization of MD blends in modern CI engines.

2 Experimental Setup and Methodology

The experiments were conducted in a single-cylinder, four-stroke, direct-injection compression ignition engine (AVL List GmbH; 5402), which was equipped with a modern common rail direct-injection (CRDI) system. The test engine was a single-cylinder version of a four-cylinder automotive high-speed direct-injection (HSDI) diesel engine. The schematic of the experimental system is shown in Fig. 1.

Detailed technical specifications of the test engine are given in Table 1.

An alternating current (AC) (transient) dynamometer (Wittur Electric Drives GmbH; 2SB 3) was used to control the engine speed and load. An open-loop fuel injection control strategy was loaded in the ETAS system to control the fuel injection parameters independently. This control system consisted of an electronic control unit, a communication interface (ETAS; ETK 7.1 Emulator probe), and a control program (INCA, a commercial tool for automotive calibration). To control the temperature of the test fuel, a fuel conditioning system (AVL; 553) was installed. For fuel flow rate measurement, a fuel-metering unit (AVL; 733S) was installed in the experimental setup, which worked on the gravimetric measurement principle. A coolant-conditioning unit (Yantrashilpa; YS4027) and a lubricating oil-conditioning unit (Yantrashilpa; YS4312) were used to control the temperatures of coolant and lubricating oil at 60 °C and 90 °C, respectively. Other details of the experimental setup can be found in our previous publication [44].

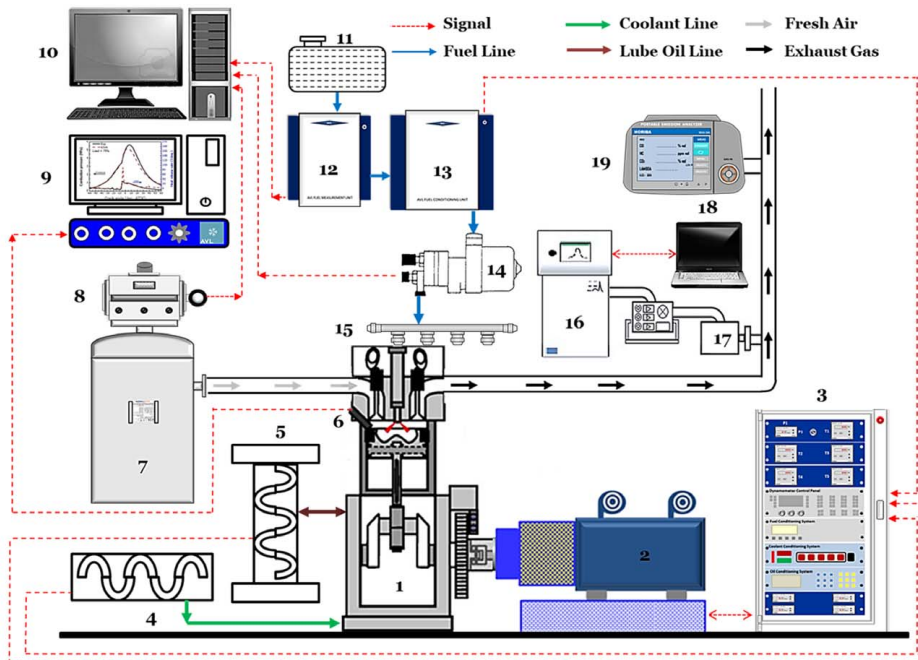
A water-cooled piezoelectric pressure transducer (AVL; QC34C) was installed in the cylinder head for data acquisition for the combustion analysis. An optical encoder (AVL; 365C) recorded the rotation of the crankshaft. In-cylinder pressure-crank angle data history was acquired and analyzed by the high-speed combustion data acquisition system (AVL; IndiMicro). An exhaust gas emission analyzer (Horiba; 584L) was used to measure the concentrations of regulated gases present in the engine exhaust. It can measure the concentrations of CO, HC, CO₂, and NO_x in the engine exhaust. The accuracy of instruments used for various measurements is given in Table 2.

For particulate measurement, an engine exhaust particle sizer (EEPS) spectrometer (TSI Inc.; 3090) was used. EEPS can measure a wide size range of particles (from 5.6 to 560 nm) with a maximum number concentration of #10⁸ particles/cm³ of the engine exhaust. A rotating disk thermo-diluter (Matter Engineering AG; MD19-2E) was used to dilute the exhaust gas before supplying it into the EEPS for particulate measurements. During the experiment, the number concentration of particles present in the diluted exhaust was measured, and a dilution factor was multiplied to calculate the actual concentration of particles emitted by the engine. Detailed specifications of EEPS can be found in our previous publication [45].

For test fuel preparation, a mechanical stirrer (Remi; RQT-124A) was used. Test fuel properties such as kinematic viscosity, calorific value, and density were determined by using a kinematic viscometer (Stanhope-Seta; 83541-3), a bomb calorimeter (Parr; 6200), and a portable density meter (Kyoto Electronics; DA130N), respectively. Table 3 shows the composition of test fuels and their physical properties. It is seen that the addition of methanol leads to a reduction in calorific value, kinematic viscosity, and density. Original properties of mineral diesel, methanol, and 1-dodecanol can be found in our previous publication [41].

Engine experiments were carried out at constant engine speed (1500 rpm) using MD10 and baseline mineral diesel. During the experiments, fuel injection quantity was varied to achieve constant engine load (3 kW). At each experimental condition, the engine was run for 30 min and the measurement of performance, emissions, and combustion-related parameters were done after thermal stabilization of the engine. Table 4 shows important experimental conditions.

For comparison of the experimental results obtained from different test fuels and fuel injection strategies, three sets of experiments were conducted as given below.



1- Single Cylinder Research Engine, 2- Transient Dynamometer, 3- Dynamometer Controller, 4- Coolant Conditioning System, 5- Lubricating Oil Conditioning System, 6- Piezoelectric Pressure Transducer, 7- Intake Air Surge Tank, 8- Air-Flow Rate Measurement System, 9- Combustion Data Acquisition System, 10- ECU Interface System, 11- Fuel Tank, 12- Fuel Measurement System, 13- Fuel Conditioning System, 14- High Pressure Fuel Pump, 15- Common Rail, 16- Engine Exhaust Particle Sizer, 17- Thermo Diluter, 18- EEPS Data Logger, 19- Exhaust gas Emission Analyzer

Fig. 1 Schematic of the experimental setup

Table 1 Specifications of the test engine

Engine make/model	AVL/5402
Number of cylinders	1
Cylinder bore/stroke	85/90 mm
Swept volume	510.7 cc
Compression ratio	17.0
Inlet ports	Tangential and swirl inlet port
Nominal swirl ratio	1.78
Maximum power/engine speed (rpm)	6 kW/4000 rpm
Fuel injection pressure	200–1400 bars
Fuel injection system	Common rail direct injection
High pressure system	BOSCH Common Rail CP 4.1
Nozzle type/diameter	DSL A 142P/180 μm
Engine management system	AVL-RPEMS + BOSCH ETK7
Valves per cylinder	4 (2 inlet, 2 exhaust)

- Case 1: Mineral diesel-fueled engine using SPI strategy
 Case 2: MD10 fueled engine using SPI strategy
 Case 3: MD10 fueled engine using DPI strategy

3 Results and Discussion

The results and discussion section is divided into three subsections, which describe engine combustion, performance and emissions, and particulate characteristics.

3.1 Combustion Characteristics. For combustion analysis, in-cylinder pressure is the most important measured parameter, which provides various calculated combustion parameters such as

Table 2 Accuracies of the measurements by various instruments

Instrument	Parameter	Accuracy
Piezoelectric pressure transducer	In-cylinder pressure	25 pC/bar
Exhaust gas emission analyzer	CO (% ν/ν)	0.01
	HC (ppm)	1
	NO _x (ppm)	1
Portable density meter	Density	0.001 g/cm ³
Kinematic viscometer	Kinematic viscosity	0.07%
Bomb calorimeter	Calorific value	0.02%

heat release rate (HRR), combustion duration, etc. For all experimental conditions, in-cylinder pressure data were acquired for an average of 250 consecutive engine cycles and then the average data set was used for further analysis. In-cylinder pressure variation and HRR variation of MD10 and mineral diesel-fueled engine at different FIPs and start of main injection (SoMI) timings are shown in Fig. 2.

In general, the in-cylinder pressure curve showed two peaks (except advanced SoMI timings), in which, the first peak corresponds to the combustion of fuel injected during pilot injection and the second peak corresponds to the combustion of fuel injected during the main injection. In-cylinder pressure trends show that advancing SoMI timing has no significant effect on the first peak; however, the second peak gets significantly advanced. Advancing SoMI timing resulted in a higher second peak for all three cases. At 6° CA bTDC (before top dead center) SoMI timing, the first peak corresponding to the pilot injection merged with the second

Table 3 Test fuels composition and important fuel properties

Test fuel	Volumetric content (% v/v)			Calorific value (MJ/kg)	Kinematic viscosity (mm ² /s) @ 40 °C	Density (g/cm ³) @ 30 °C	Surface tension (mN/m) @ 40 °C ^a
	Diesel	Methanol	1-Dodecanol				
Diesel	100	–	–	44.26	2.96	0.837	23.619
MD10	89	10	1	43.12	2.79	0.829	23.507

^aValues taken from the literature.

Table 4 Experimental conditions

Engine speed	1500 rpm
Test fuels	Diesel and MD10
Fuel injection pressure	500, 750, and 1000 bars
Fuel injection strategy	With SPI and DPI along with main injection
Pilot injection timings	(SoPI) ₁ = 30° CA bTDC (SoPI) ₂ = 20° CA bTDC
Main injection timings	–3 deg, 0 deg, 3 deg, and 6° CA bTDC

peak. More time availability for fuel-air mixing at advanced SoMI timings was the main reason for this trend, which became more prominent at higher FIPs. HRR trends also showed similar behavior. Increasing FIP affected both the peaks of in-cylinder pressure and advanced the combustion. This was primarily attributed to improved fuel-air mixing due to superior fuel spray atomization at higher FIPs.

Higher FIP also resulted in a higher HRR peak, which showed faster heat release due to improved fuel-air combustion kinetics. A comparison of two test fuels (mineral diesel and MD10) showed that mineral diesel-fueled engine resulted in earlier combustion compared with MD10. Lower CN of MD10 might be a possible reason for this behavior, which causes longer ignition delay. Advancing SoMI timing enhances this behavior slightly due to the dominating effect of ignition delay at advanced SoMI timings. MD10 exhibited a slightly higher maximum HRR compared with mineral diesel. Increasing FIP showed an interesting behavior. At higher FIPs, MD10 exhibited advanced combustion compared with mineral diesel, which subsequently retarded with advancing SoMI timing. At higher FIP, retarded SoMI timing showed two distinct peaks, which merged into a single peak for advanced SoMI timings. HRR trends showed that combustion at advanced SoMI timings and higher FIPs resulted in a relatively shorter duration for the main combustion event. Among both test fuels, a relatively smaller width of the HRR

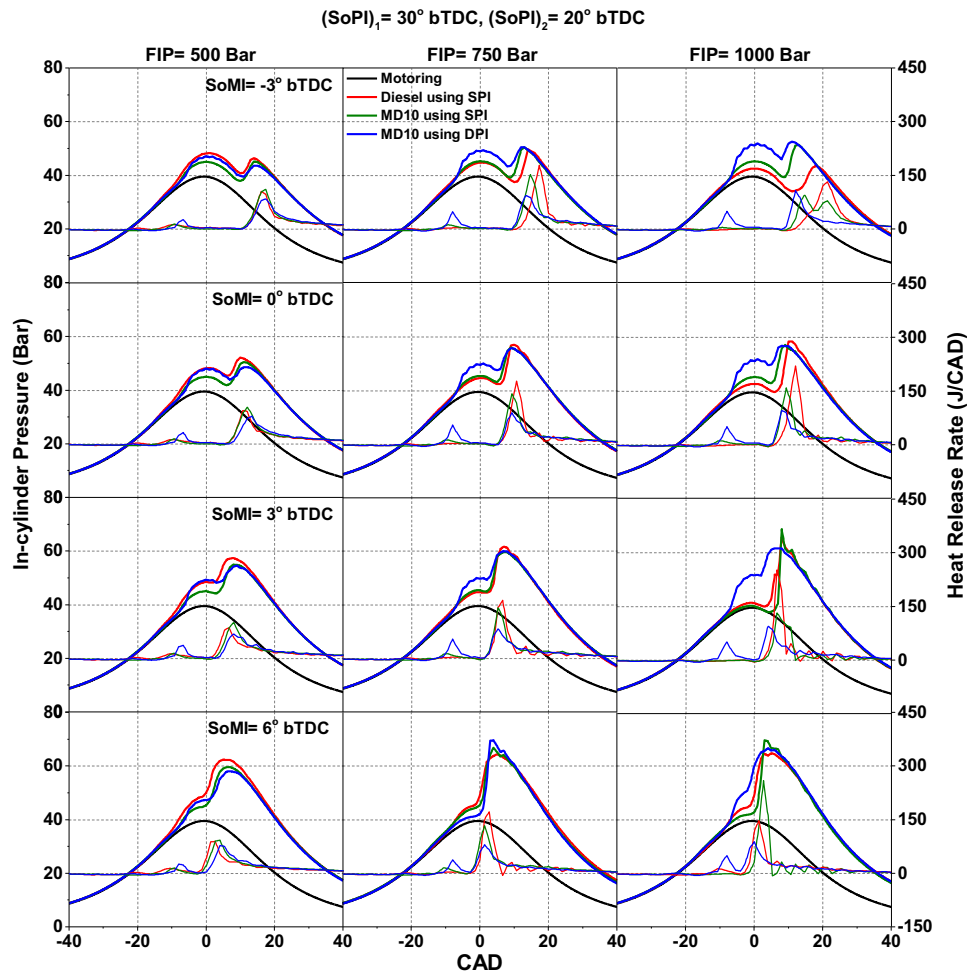


Fig. 2 In-cylinder pressure and HRR variation with respect to crank angle position for MD10 and mineral diesel-fueled engines using different fuel injection strategies

curve corresponding to mineral diesel showed a slightly shorter combustion duration. This was attributed to a relatively lower burning velocity of MD10 compared with mineral diesel [32]. At higher FIPs, knocking behavior was clearly seen in HRR curves, which further enhanced with advancing SoMI timings. Among both test fuels, MD10 showed slightly more knocking behavior than mineral diesel. To resolve this issue, DPI strategy was used for MD10, which showed a relatively more stable combustion of MD10 compared with the SPI strategy. In the case of DPI strategy, the in-cylinder pressure increased gradually before the SoC, which eliminated knocking hence resulted in smoother combustion. At lower FIP, DPI strategy behaved similarly to SPI strategy and resulted in relatively inferior combustion, however at higher FIPs, DPI strategy resulted in superior combustion. In the DPI strategy, the difference between the two peaks of in-cylinder combustion curves also approached closer to each other, which improved the combustion.

3.2 Performance and Emission Characteristics. Experiments were conducted to compare the performance parameters, namely, brake thermal efficiency (BTE), BSEC, and exhaust gas temperature (EGT) at different FIP and SoMI timings.

Figure 3 showed that advancing SoMI timings resulted in lower BTE for both test fuels. This was mainly due to advanced combustion phasing, which resulted in lower piston work. Increasing FIP improved the BTE of both test fuels; however, too high FIP slightly deteriorated the BTE (Fig. 3(c)). BTE reduction was more significant at lower FIP (500 bars) because of combined effects of two deteriorating factors, namely: (i) inferior fuel atomization at lower FIPs and (ii) lower in-cylinder temperature and pressure conditions at too advanced SoMI timings. At higher FIP (1000 bars), reduction in BTE at advanced SoMI timing was slightly higher than that at 750 bars FIP. Impingement of spray on to the cylinder walls and piston cavity might be responsible for lower BTE at advanced SoMI timings. A shift in BTE for all three cases is an important

observation of this study. At lower FIP, mineral diesel showed higher BTE compared with MD10. At 750 bars, MD10 resulted in higher BTE compared with mineral diesel however at 1000 bars, both test fuels exhibited slightly lower BTE compared with 750 bars. This issue was resolved by DPI strategy, which showed relatively inferior performance at lower FIP, however DPI strategy resulted in improved performance at higher FIP. At higher FIP, DPI strategy reduced the fuel spray impingement on the piston and avoided over leaning of fuel-air mixture, which improved the combustion. At 1000 bars FIP, DPI strategy fueled with MD10 resulted in $\sim 33.5\%$ BTE. BSEC followed almost similar performance trends as that of BTE. At 750 bars, all three cases resulted in almost similar BSEC except the most advanced SoMI timing. However, at 500 bars FIP, mineral diesel and at 1000 bars FIP, MD10 using DPI strategy exhibited the lowest BSEC. Guo et al. [36] reported that MD blends exhibited relatively higher BSFC compared with baseline mineral diesel. EGT was another important performance parameter measured in this study. EGT is an indirect measure of bulk in-cylinder combustion temperature. For both test fuels, EGT decreased with advancing SoMI timing. This reflects that advancing SoMI timing improved the fuel-air mixing, leading to enhanced premixed combustion compared with diffusion combustion. Similarly, increasing FIP also led to lower EGT. At higher FIP, overall combustion duration decreased, which resulted in lower EGT. At 500 bars, both test fuels showed almost similar EGT however DPI strategy with MD10 resulted in lower EGT compared with SPI strategy. This showed that DPI strategy improved the premixed combustion and resulted in reduced EGT. At 750 bars, MD10 resulted in lower EGT compared with mineral diesel. At 750 bars, MD10 using both SPI and DPI strategies resulted in almost similar EGT. At 1000 bars FIP, all three conditions were different in terms of EGT and the effect of fuel properties and injection parameters were clearly visible. Mineral diesel exhibited higher EGT compared with MD10 using SPI strategy. In addition, the DPI strategy resulted in lower EGT compared with SPI strategy.

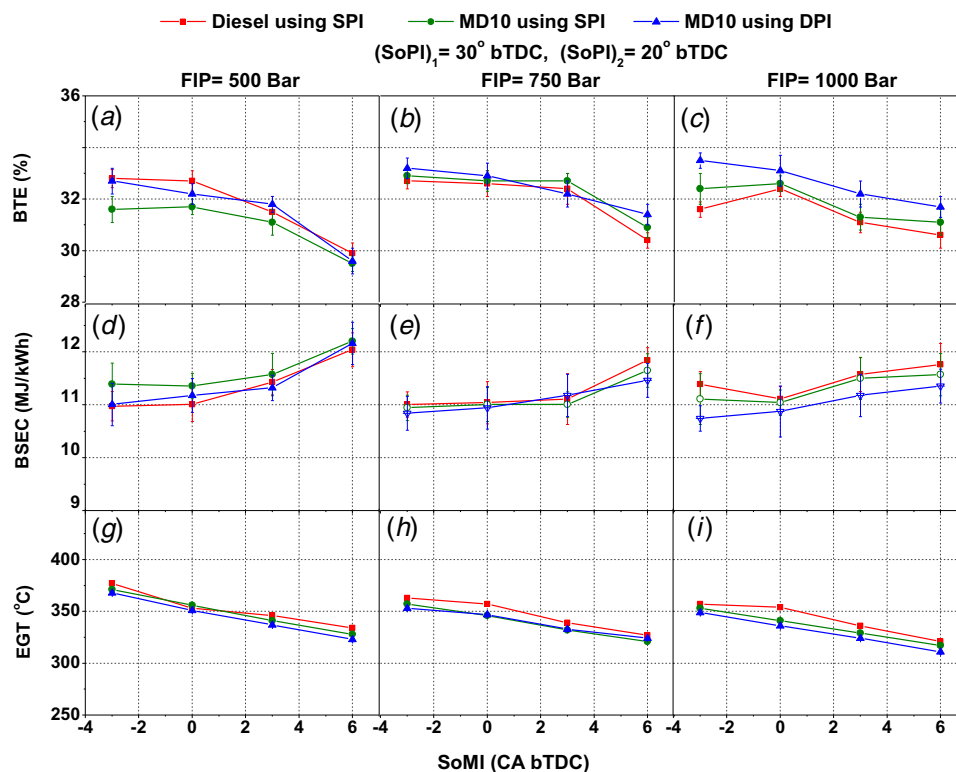


Fig. 3 BTE, BSEC, and EGT of MD10 and mineral diesel-fueled engines using different fuel injection strategies

Figure 4 shows the emissions of HC, CO, and NO_x . Gas emission concentrations of these pollutant species were measured and then converted into brake-specific emissions (in g/kWh) using standard methodology [46].

Figure 4 shows that the difference between brake-specific HC emissions at different FIPs was not significant, except at advanced SoMI timings. At advanced SoMI timings (especially at 6° CA bTDC), combined effects of factors such as spray impingement on the cylinder walls and piston cavity, and relatively inferior in-cylinder conditions led to slightly higher HC emissions compared with retarded SoMI timings. At 500 bars FIP, retarded SoMI timings resulted in slightly higher HC emissions. However, at advanced SoMI timings, brake-specific HC emissions remained constant for both test fuels. At lower FIP, mineral diesel exhibited lower HC emissions compared with MD10 however at 1000 bars FIP, mineral diesel exhibited slightly higher HC emissions compared with MD10. This variation of HC emissions may be due to the wall-quenching effect of methanol. Due to lower heating value and higher charge cooling effect of methanol, MD10 exhibited relatively lower flame temperatures and lower burning velocities compared with mineral diesel, which led to a greater degree of incomplete combustion. Sayin et al. [41] also reported slightly higher HC emissions from engine fuelled with MD blends, especially at retarded SoI timings. Between two pilot injection strategies, the DPI strategy was more effective in HC emission reduction at 1000 bars FIP, however at lower FIPs, SPI strategy was found to be more effective. CO emission also followed a trend similar to HC emissions. Brake-specific CO emission also did not show any significant variation at different SoMI timings and FIPs. Mineral diesel exhibited relatively lower CO emission compared with MD10. Between the fuel injection strategies, the DPI strategy was found to be more effective up to 750 bars FIP, however at 1000 bars FIP, DPI strategy resulted in higher CO emission compared with SPI strategy. Relatively lower EGT might be a possible reason for this, which prevented oxidation of CO into CO_2 and resulted in higher emission of CO. For both test fuels, advancing SoMI timing did not show any significant variation in NO_x

emissions however increasing FIP resulted in slightly higher NO_x emissions. Although Sayin et al. [41] reported that NO_x emissions from the engine fuelled with MD blends slightly increased with advancing SoMI timings. In this study, mineral diesel emitted higher NO_x compared with MD10. Relatively lower in-cylinder temperatures of MD10 engine compared with mineral diesel engine might be a possible reason for this. Among the two pilot injection strategies, DPI strategy was more effective in NO_x reduction. At all FIPs, the DPI strategy resulted in lower NO_x emissions compared with SPI strategy. This finding correlates very well with the engine performance results, which suggested that the DPI strategy resulted in relatively lower EGT compared with the SPI strategy.

Figure 5 shows the correlation between BTE and NO_x emissions at different SoMI timings and FIPs. For each test fuel and fuel injection strategy, BTE is shown by lines and NO_x emissions are shown by the background color. For each test fuel, overlapping of minimum NO_x emissions zone and maximum BTE (optimum zone, shown by hatching pattern) gives an optimum range of fuel injection parameters. For mineral diesel, a very small range of FIPs and SoMI timings were found for the highest BTE ($\sim 32.4\%$) and most of the fuel injection strategies showed higher NO_x emissions. With increasing FIP, SoMI timing for optimum zone varied in a random pattern. Compared with mineral diesel, MD10 showed a relatively wider optimal zone, which was located at medium FIP (~ 750 bars) and intermediate SoMI timings (~ 3 to -3° CA bTDC). Optimum zone for MD10 using SPI strategy showed $\sim 32.5\%$ BTE and relatively lower NO_x emissions compared with mineral diesel. MD10 using the DPI strategy was found to be the best amongst three cases. This gives a wider optimum zone, in which maximum BTE was $\sim 33\%$ and NO_x was the lowest amongst the three cases. This correlation map showed that the DPI strategy was suitable at higher FIP and retarded SoMI timings (~ 2 to -1° CA bTDC).

3.3 Particulate Characteristics. Particulate investigations are an important part of this study. Most particulates emitted by diesel

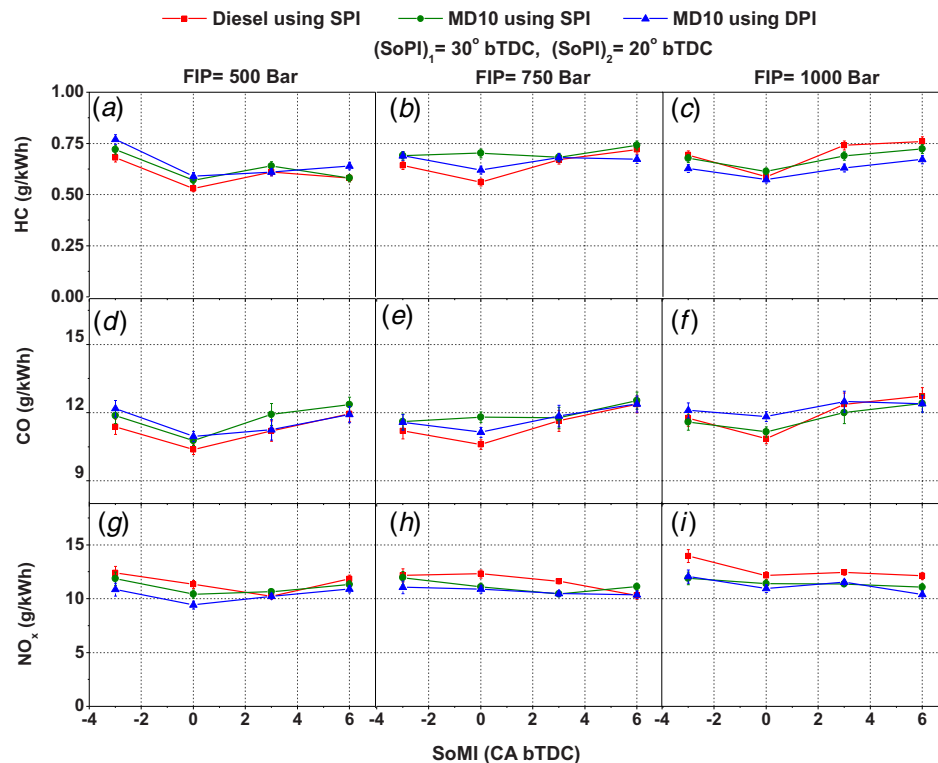


Fig. 4 Brake-specific emissions of CO, HC, and NO_x emitted from MD10 and mineral diesel-fueled engines using different fuel injection strategies

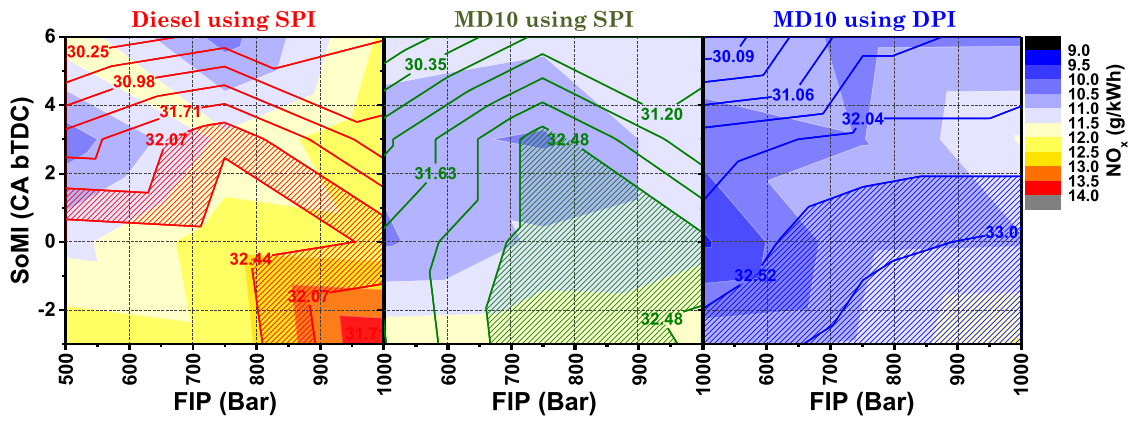


Fig. 5 BTE (shown by contour lines) and NO_x (shown by background contour) emitted by MD10 and mineral diesel-fueled engines using different fuel injection strategies

engines are formed due to heterogeneous fuel-air mixing, wherein soot precursors are generated in the fuel-rich (oxygen deficit) zones. This study attempted to address these issues by using oxygenated additives and pilot fuel injection strategy. Pilot injection results in the more homogenous fuel-air mixture formation and the fuel-bound oxygen promotes fuel oxidation in the fuel-rich zones of the combustion chamber. To gain deeper insights into the effect of these parameters

on particulate emissions, the experiments were performed using different test fuels, different fuel injection strategies, and varying the fuel injection parameters. Therefore this section is divided into three subsections, namely, number-size, surface area-size, and mass-size distributions of particulates. In each sub-section, particulate characteristics were described based on their size (mobility diameter, D_p) and are classified as nanoparticles (NP, $D_p < 10$ nm), nucleation mode particles

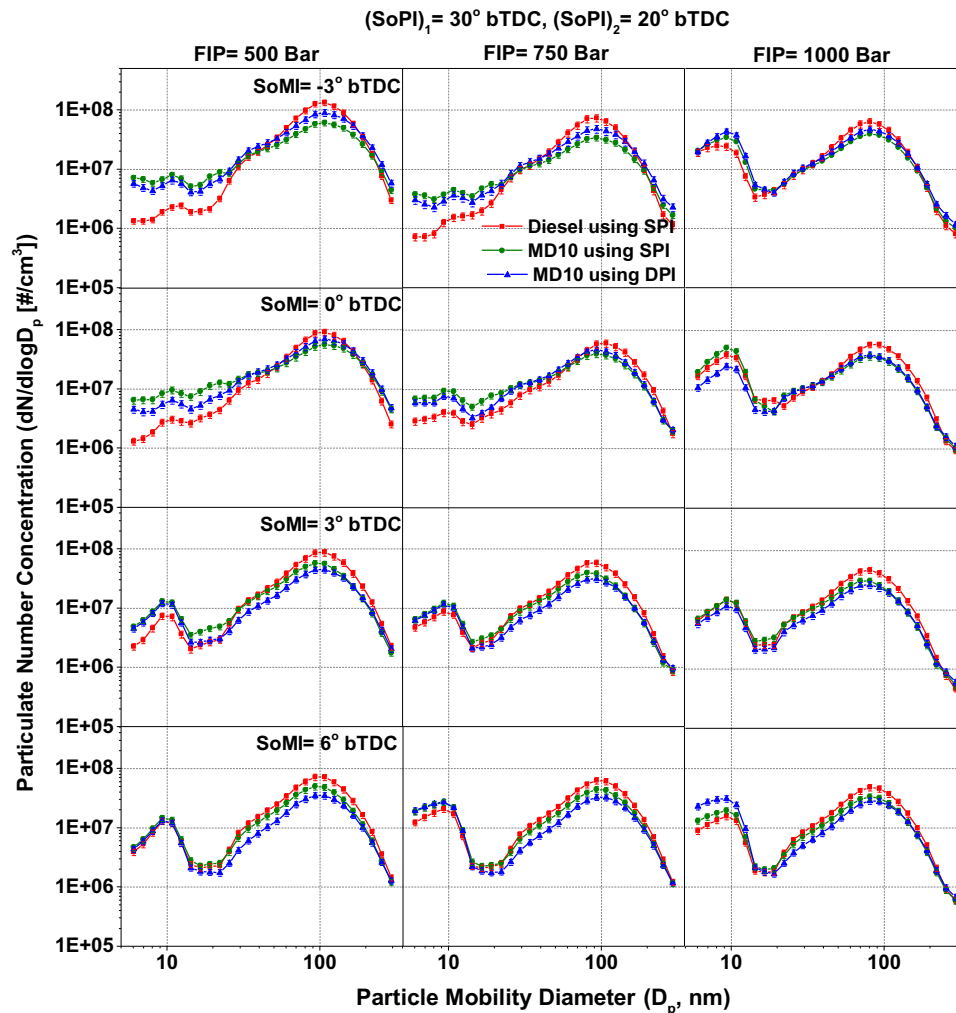


Fig. 6 Number-size distribution of particulates emitted by MD10 and mineral diesel-fueled engines using different fuel injection strategies

(NMP, $10 \text{ nm} < D_p < 50 \text{ nm}$), and accumulation mode particles (AMP, $50 \text{ nm} < D_p < 1000 \text{ nm}$) [47].

Figure 6 shows the number-size distribution of particulates emitted from MD10 and mineral diesel-fueled engines using different fuel injection strategies. The number-size distribution of particulates was calculated by the following formula [48].

$$n = \frac{c \varphi}{tQ\eta}$$

where n = number weighted concentration per channel; c = particle counts per channel; φ = sample dilution factor; t = sampling time; Q = sample flow rate; and η = sample efficiency factor per channel.

For all test fuels, advancing SoMI timing resulted in a lower peak of the particulate number-size distribution. With advancing SoMI timings, the number-size distribution changed from unimodal (peak in AMP region) to bimodal (peaks in NP and AMP region distribution). This revealed that advancing SoMI timing promoted the NP emissions. At advanced SoMI timings, a higher number of NPs and lesser number of NMPs and AMPs were emitted, which was attributed to the availability of more time for fuel-air mixing as well as relatively milder in-cylinder conditions (temperature and pressure).

For all test fuels, increasing FIP resulted in decreasing particulate number concentrations. This was mainly due to improved fuel atomization at higher FIPs, which led to more homogeneous fuel-air mixture formation. This resulted in lower particulate formation [49]. Increasing FIP shifted the peak of the number-size

distribution curve towards smaller sizes, which depicted that increasing FIP led to relatively lesser condensation of volatile species hence relatively smaller particulate formation. The relatively higher number concentration of NPs was another important observation of this study. At higher FIPs, shifting of number-size distribution from unimodal to bimodal nature showed that the effect of SoMI timings was more dominant at higher FIPs. A comparison of the two test fuels showed that MD10 resulted in a slightly higher number concentration of smaller particles (NPs and NMPs) and a lower concentration of AMPs compared with mineral diesel. Shore et al. [37] also reported that engine fuelled with MD blends exhibited lower particulate emissions than that of baseline mineral diesel. The presence of fuel-bound oxygen in MD10 promoted oxidation by modifying the local fuel-air ratio, which might be a possible reason for relatively lesser AMPs. The presence of methanol in test fuel also improves the atomization characteristics of fuel spray due to its relatively lower viscosity compared with mineral diesel. Oxygen present in MD10 produces OH radicals, which effectively enhance oxidation of diesel spray and reduce particle/soot precursor formation in the diffusion combustion phase. With increasing FIP and advancing SoMI timings, the difference in the NP number concentrations between MD10 and mineral diesel reduced. This was mainly due to improved fuel atomization and time available, which improved the fuel-air mixture formation. The effect of fuel-air mixing on particulate emissions was also investigated using the DPI strategy. Comparison of particulate characteristics from the MD10 fueled engine under SPI and DPI

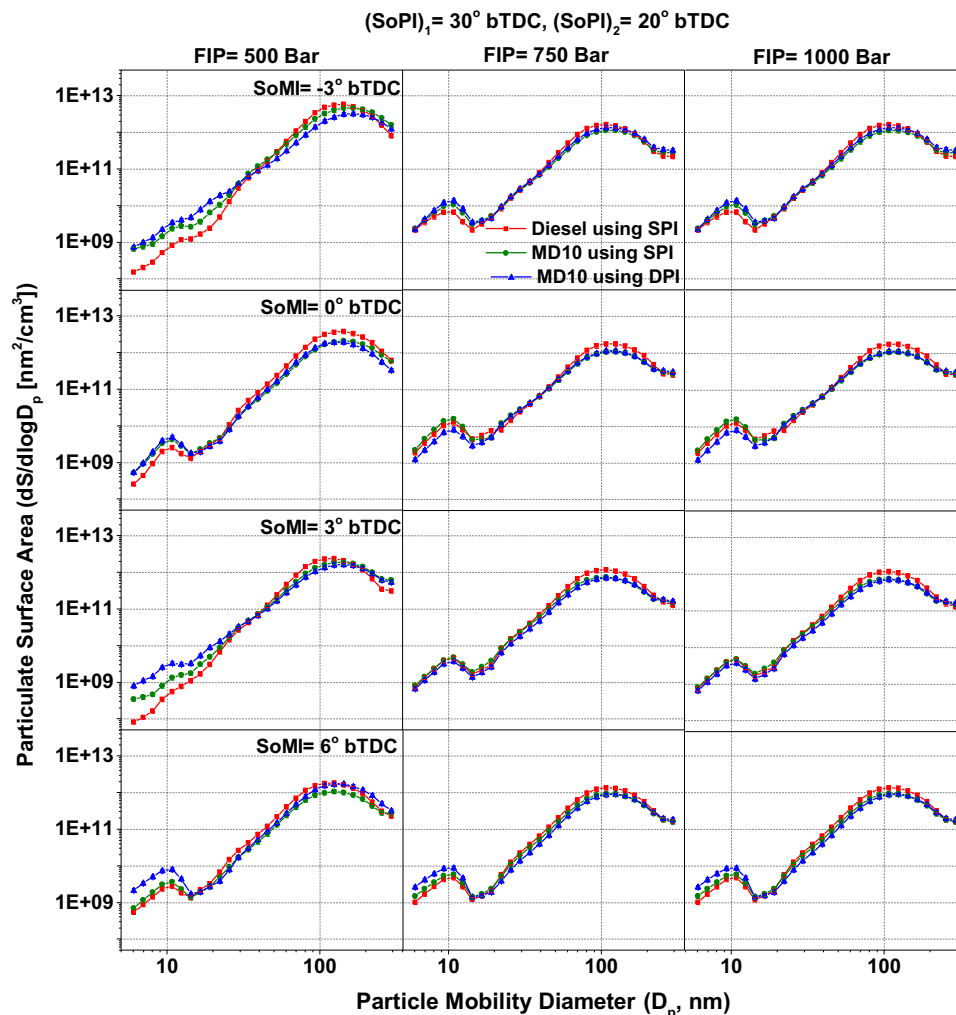


Fig. 7 Surface area-size distribution of particulates emitted by MD10 and mineral diesel-fueled engines using different fuel injection strategies

strategies showed that DPI strategy resulted in lesser AMPs and NPs at advanced SoMI timings [47]. This was mainly due to prolonged ignition delay at advanced SoMI timings, which promoted the premixed combustion. In the DPI strategy, presence of more fuel quantity before the main injection increased the in-cylinder temperature and pressure, leading to improved combustion of the fuel injected during the main injection. Improved fuel-air mixing in DPI strategy hampered the diffusion combustion, where most AMPs are generated generally. Effect of DPI strategy was less effective at retarded SoMI timings though.

Figure 7 shows the surface area-size distribution of particulates emitted by MD10 and mineral diesel-fueled engines using different fuel injection strategies.

The particle surface area-size distribution was calculated using the following formula [48]:

$$s = \pi D_p^2 n$$

where s = surface area-weighted concentration per channel; D_p = particle diameter (channel mid-point); and n = number weighted concentration per channel. Particulate surface area-size distribution is an important parameter related to particulate emissions because it affects the toxicity as well as potential health hazards to the human health [1,50]. From previous studies, it clearly emerges that smaller particulates are more harmful because they can penetrate deeper into the human respiratory system and they have higher retention in the alveolar region of lungs [1,50,51]. Relatively higher

surface area to mass ratio of smaller particulates also increases the availability of adsorption sites for condensation of toxic species such as polycyclic aromatic hydrocarbons, thus rendering them to be more toxic than larger particulates.

Results showed that advancing SoMI timing lowered the peak of particulate surface area-size distribution. The tendency of bimodal distribution was also seen at the most advanced SoMI timing (6° CA bTDC). This showed that advanced SoMI timing was not suitable from a particulate emissions point of view. Similar to number-size distribution, particulate surface area-size distribution also decreased with increasing FIP. This shows that increasing FIP reduces the surface area of particulates, which is beneficial from a particulate toxicity point of view. When FIP increased from 500 bars to 750 bars, a significant effect on particulate characteristics was observed, however further increase in FIP from 750 bars to 1000 bars did not show any notable difference in particulate characteristics. Among the two test fuels, MD10 showed relatively lower particulate surface area (corresponding to AMP region) and slightly higher surface area (corresponding to NP and NMP regions). At higher FIPs, the difference in surface area of particulates emitted from MD10 and mineral diesel became almost the same. Particulate surface area distribution showed that the DPI strategy was not very useful in the reduction of particulate surface area distribution. During most operating conditions, the SPI strategy exhibited slightly lower particulate surface area distribution compared with the DPI strategy.

Figure 8 shows the mass-size distribution of particulates, which was calculated directly by assuming particle shape as spherical

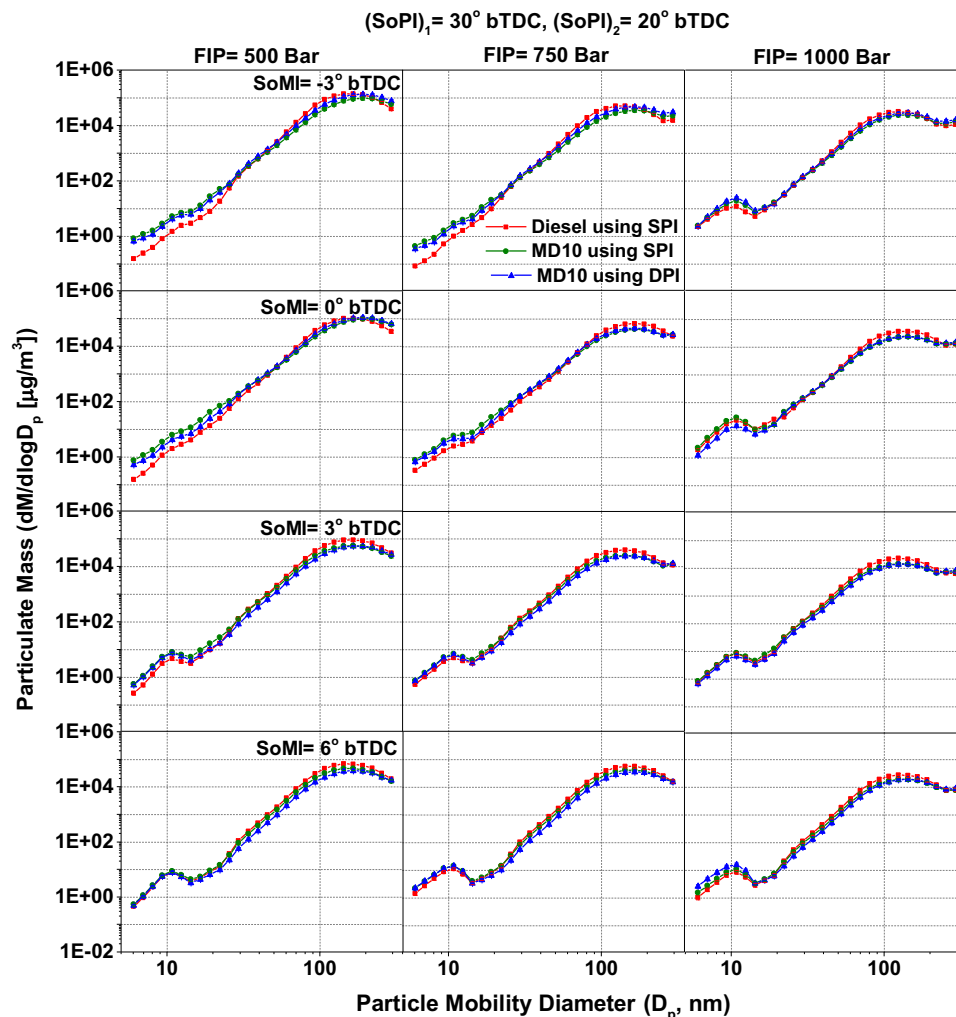


Fig. 8 Mass-size distribution of particulates emitted by MD10 and mineral diesel-fueled engines using different fuel injection strategies

and particle density to be constant. Particulate mass was calculated using the following formula [48]:

$$m = \rho v$$

where m = mass-weighted concentration per channel; ρ = particle density; and v = volume-weighted concentration per channel.

Mass-size distribution is also a very important characteristic of particulates because it affects the probability of their inhalation by human beings. Lighter particulates have longer atmospheric retention time, which increases the probability of their inhalation by the humans. On the other hand, heavier particulates settle down rather quickly. Particulate mass-size distribution followed a similar trend as that of surface area-size distribution. Particulate mass-size distribution got lowered by advancing SoMI timings and increasing FIP. The tendency of particulates of smaller size increased with advancing SoMI timing and increasing FIP. Amongst the two test fuels, MD10 exhibited relatively lower mass-size distribution compared with mineral diesel. Two fuel injection strategies (SPI and DPI) did not show a significant difference in the mass-size distribution of particulates.

For a detailed analysis of particulates, statistical analysis of particulate number-size distribution was also done. Particulate number concentration corresponding to each region was calculated using the following equation [48]:

$$N = \sum_l^u n$$

where N = total number concentration, l = lower channel boundary, u = upper channel boundary, and n = number weighted concentration per channel. For each region, number concentration was calculated by varying l and u as given below [45]

NP: $l = 5.6$ nm and $u = 10$ nm

NMP: $l = 10$ nm and $u = 50$ nm

AMP: $l = 50$ nm and $u = 560$ nm

Total particulate number (TPN): $l = 5.6$ nm and $u = 560$ nm.

Figure 9 shows the variation of NP, NMP, and AMP number concentrations emitted by MD10 and mineral diesel-fueled engines using different fuel injection strategies. These results validated the findings of particulate number-size distributions (Fig. 6). It can be clearly seen from Fig. 9 that most particulates emitted by CI engines were in the AMP region. Advancing SoMI timing and increasing FIP resulted in higher NP and NMP number concentrations however AMP number concentration slightly decreased. At 1000 bars FIP, NP, NMP, and AMP number concentrations became almost the same and NP and NMP number concentration at different SoMI timings showed a slight deviation from their regular trend.

This statistical analysis showed that MD10 fueled engine emitted slightly higher NPs and NMPs compared with mineral diesel-fueled engine, however AMPs from MD10 were significantly lower compared with mineral diesel. The use of the DPI strategy showed a random pattern of NPs, NMPs, and AMPs. DPI strategy resulted in the emission of a lower number of particulates compared with mineral diesel, however this strategy was found to be less effective compared with SPI strategy.

Figure 10 shows the comparison of TPN vs. count mean diameter (CMD) of particulates emitted by MD10 and mineral diesel-fueled engines using different fuel injection strategies.

CMD gave a better interpretation of engine-out particulate emissions and their adverse health effects. CMD decreased consistently with advancing SoMI timing for 500 and 750 bars FIP. However, these trends were not consistent for 1000 bars FIP. CMD decreased with advancing SoMI timing, mainly due to a relatively higher number concentration of smaller particles. TPN concentration decreased with increasing FIP. This reduction was significant up to intermediate FIP, however too high FIP (1000 bars) showed TPN reduction only in case of advanced SoMI timings. For good particulate emission characteristics, total particulate mass (TPM) should be low and CMD should be large because smaller CMD provides greater surface area per unit mass of particulates for adsorption of toxic compounds [1].

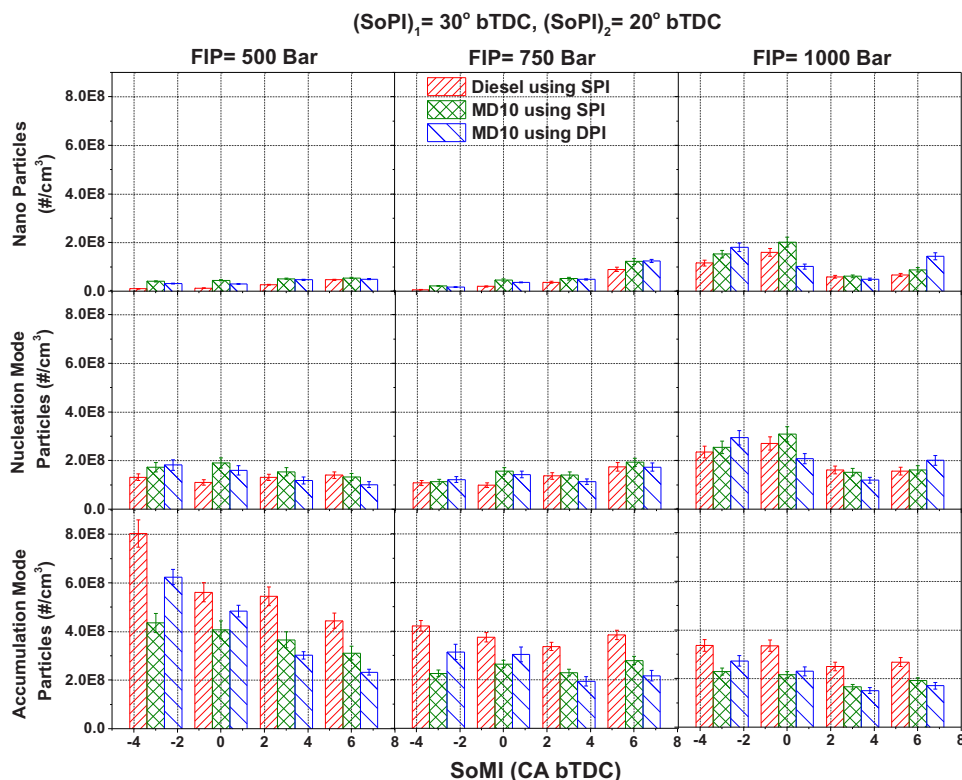


Fig. 9 NP, NMP, and AMP number concentrations emitted by MD10 and mineral diesel-fueled engines using different fuel injection strategies

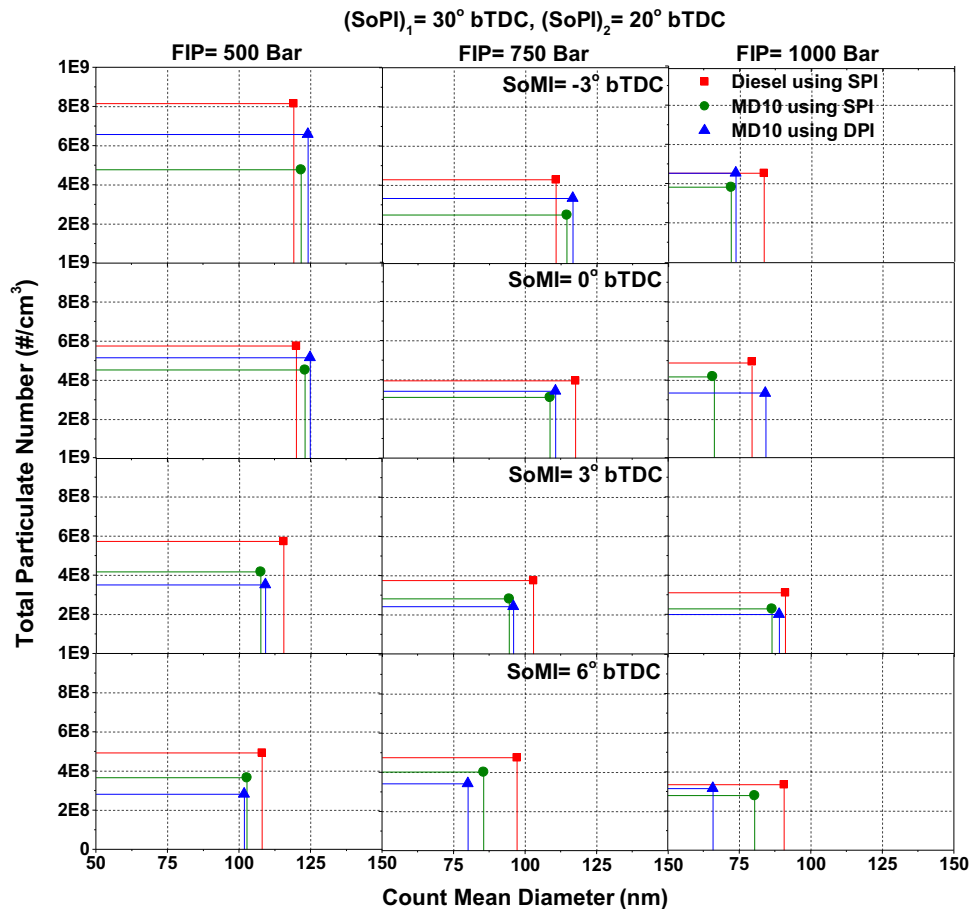


Fig. 10 Correlation between TPN and CMD of particulates emitted by MD10 and mineral diesel-fueled engines using different fuel injection strategies

Figure 11 shows the number-mass correlation of particulates emitted by MD10 and mineral diesel-fueled engines using different fuel injection strategies. Smaller particulates contribute less to the particulate mass, however their contribution in particulate number concentration cannot be neglected. Bigger particles contribute significantly to the particulate mass however they are relatively less harmful to the environment and human health compared with smaller NPs [1]. Hence, it is desirable to establish a relationship/correlation between the particulate mass and particulate number-size distributions [52]. In this analysis, particulate mass is shown on the Y-axis and particulate numbers are shown on the X-axis. A lobe was plotted by joining the particulate number and mass corresponding to each mean particulate size in an increasing size ranging from 5.6 to 560 nm. The size of the lobe reflects the relationship between the particulate mass and particulate numbers. Larger lobe indicates higher particulate emissions in terms of both, numbers as well as mass. If the lobe is inclined toward the X-axis, this indicates dominance of particulates numbers. If this lobe is inclined toward the Y-axis, it indicates the dominance of particulate mass. This lobe reflects the lower contribution of smaller sized particles to the particulate mass and vice versa.

In this analysis, the lobe of particulates emitted by the mineral diesel-fueled engine was relatively larger compared with MD10 at all the engine operating conditions. Lobe size reduced with advancing SoMI timing as well as with increasing FIP. There was no significant difference in the inclination of SoMI timing towards either the particulate number or particulate mass axis. At higher FIPs, an inclination of these lobes increased towards the X-axis, which signifies that particulate numbers start dominating at higher FIPs, however their contribution to the particulate

mass was insignificant. The use of two injection strategies showed that particulate characteristics of DPI strategy were inferior at lower FIPs and at retarded SoMI timings. It reflects that the fuel injection strategy should be varied based on the fuel injection parameters.

Figure 12 shows a correlation between TPM and NO_x emitted by MD10 and mineral diesel-fueled engines using different fuel injection strategies. Particulate number concentration corresponding to each region was calculated using the following equation [48]:

$$M = \sum_l^u m$$

where M = TPM, l = lower channel boundary, u = upper channel boundary; and m = particulate mass per channel. For each fuel, the overlapped area between SoMI, FIP, and total particle mass shows the optimum zone.

Results showed that optimum zones of mineral diesel and MD10 using SPI strategy were almost similar in terms of fuel injection parameters. For both cases, advanced SoMI timings (2° to 6° CA bTDC) at higher FIPs resulted in lower TPM and NO_x emissions. In the optimum zone, MD10 showed relatively lower TPM ($\sim 1.8 \times 10^5 \mu\text{g}/\text{m}^3$) and NO_x ($\sim 10 \text{ g}/\text{kWh}$) compared with mineral diesel, which were ($\sim 2.5 \times 10^5 \mu\text{g}/\text{m}^3$) and ($\sim 13 \text{ g}/\text{kWh}$), respectively. MD10 using DPI strategy exhibited a slightly narrower optimum zone compared with the previous two cases. DPI strategy resulted in slightly higher TPM ($\sim 2.0 \times 10^5 \mu\text{g}/\text{m}^3$) compared with SPI strategy, however this strategy was found to be more effective for NO_x reduction.

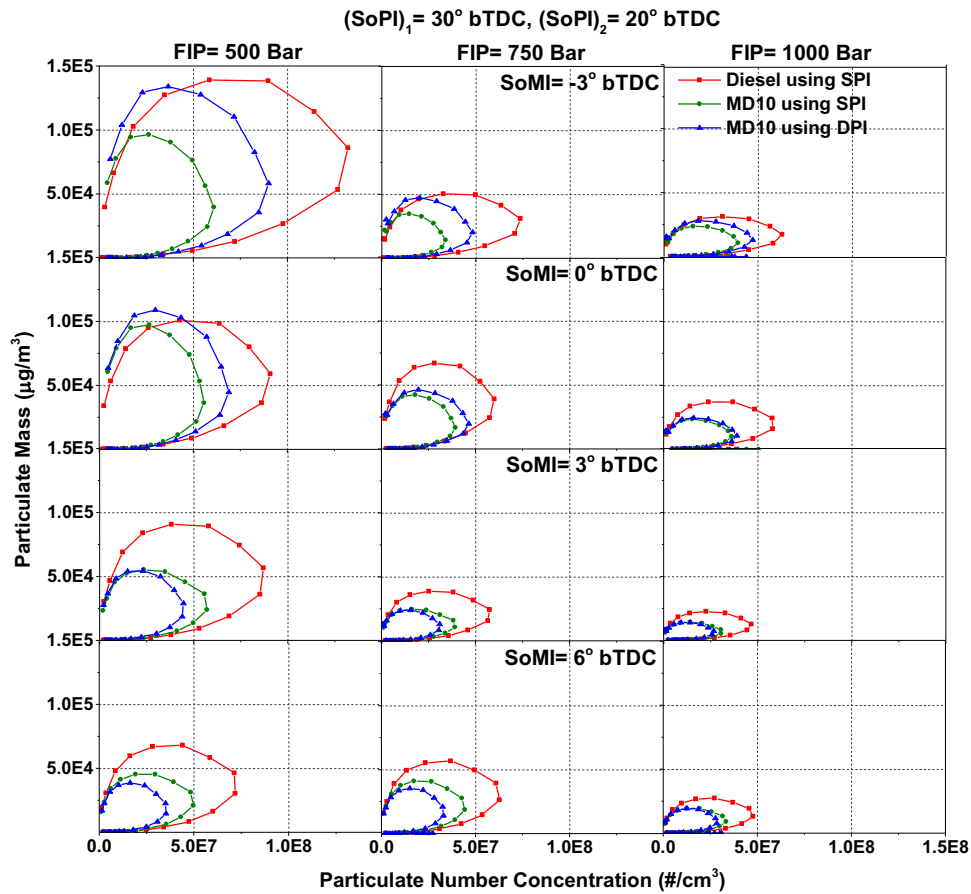


Fig. 11 Correlation between number and mass-size distribution of particulates emitted by MD10 and mineral diesel-fueled engines using different fuel injection strategies

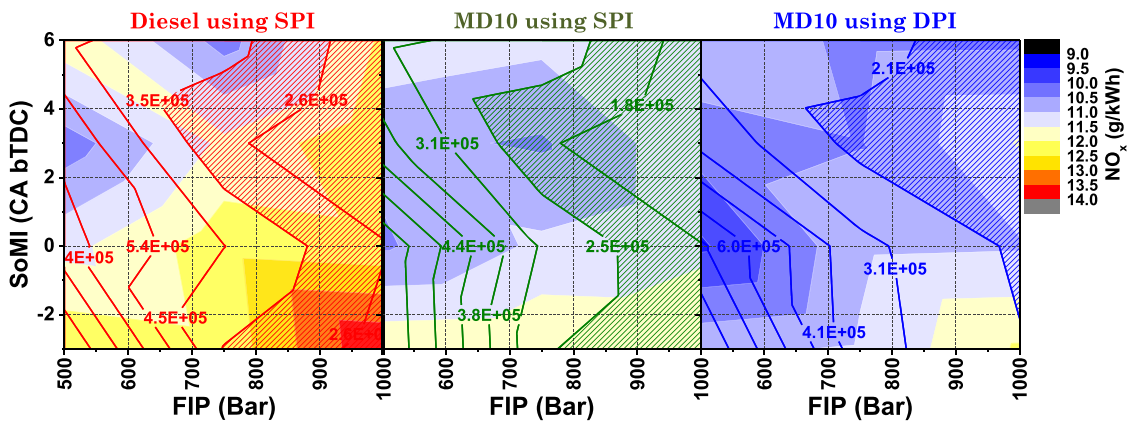


Fig. 12 Correlation between TPM ($\mu\text{g}/\text{m}^3$ of exhaust gas shown by contour lines) and NO_x (shown by background contour) emitted by MD10 and mineral diesel-fueled engines using different fuel injection strategies

4 Conclusions

In this study, MD10 (10% (v/v) methanol blended with mineral diesel) and baseline mineral diesel were utilized in a single-cylinder research engine. The experiments were conducted using two fuel injection strategies namely SPI and DPI at different FIPs and SoMI timings. Results showed that the addition of methanol in mineral diesel retarded the combustion events at lower FIP and resulted in advanced combustion at higher FIPs. The effect of increasing FIP was more dominant in MD10 compared with mineral diesel and it improved both, the combustion and the performance characteristics. At higher FIPs, DPI strategy improved the

combustion, leading to higher BTE, lower EGT, and reduced NO_x emissions. MD10 using SPI strategy yielded lower particulates compared with mineral diesel and DPI strategy was found to be less effective in particulate emission reduction. The higher number concentration of smaller particulates (NPs and NMPs) from the MD10 fueled engine was an important observation of this study. The particulate number-mass analysis showed that increasing FIP and advancing SoMI timings resulted in lower particulate mass emissions. TPM- NO_x correlation showed that suitable fuel injection parameters are critical for achieving particulate- NO_x trade-off in modern engines and should be carefully analyzed.

Acknowledgment

The authors would like to acknowledge the efforts of Dr. Nirendra N. Mustafi, Post-doctoral fellow at ERL, for his assistance in the proof-reading of the manuscript.

References

- Agarwal, A. K., Ateeq, B., Gupta, T., Singh, A. P., Pandey, S. K., Sharma, N., Agarwal, R. A., Gupta, N. K., Sharma, H., Jain, A., and Shukla, P. C., 2018, "Toxicity and Mutagenicity of Exhaust From Compressed Natural Gas: Could This be a Clean Solution for Megacities With Mixed-Traffic Conditions?," *Environ. Pollut.*, **239**, pp. 499–511.
- Gandhidasan, P., Ertas, A., and Anderson, E. E., 1991, "Review of Methanol and Compressed Natural Gas (CNG) as Alternative for Transportation Fuels," *ASME J. Energy Resour. Technol.*, **113**(2), pp. 101–107.
- Agarwal, A. K., Singh, A. P., Gupta, T., Agarwal, R. A., Sharma, N., Rajput, P., Pandey, S. K., and Ateeq, B., 2018, "Mutagenicity and Cytotoxicity of Particulate Matter Emitted from Biodiesel-Fueled Engines," *Environ. Sci. Technol.*, **52**(24), pp. 14496–14507.
- Sharma, N., and Agarwal, A. K., 2020, "Effect of Fuel Injection Pressure and Engine Speed on Performance, Emissions, Combustion, and Particulate Investigations of Gasohols Fueled Gasoline Direct Injection Engine," *ASME J. Energy Resour. Technol.*, **142**(4), p. 042201.
- Oldenkamp, R., van Zelm, R. V., and Huijbregts, M. A. J., 2016, "Valuing the Human Health Damage Caused by the Fraud of Volkswagen," *Environ. Pollut.*, **212**, pp. 121–127.
- Hu, G., Liao, S., Zuo, Z., Wang, K., and Zhu, Z., 2018, "Kinetic Effects of Methanol Addition on the Formation and Consumption of Formaldehyde and Benzene in Premixed n-Heptane/Air Flames," *ASME J. Energy Resour. Technol.*, **140**(7), p. 072205.
- He, B. Q., Shuai, S. J., Wang, J. X., and He, H., 2003, "The Effect of Ethanol Blended Diesel Fuels on Emissions From Diesel Engine," *Atmos. Environ.*, **37**(35), pp. 4965–4971.
- de Caro, P. S., Mouloungui, Z., Vaitilingom, G., and Berge, J. C., 2001, "Interest of Combining an Additive With Diesel-Ethanol Blends for Use in Diesel Engines," *Fuel*, **80**(4), pp. 565–574.
- Yoon, S. H., Park, S. H., Suh, H. K., and Lee, C. S., 2010, "Effect of Biodiesel-Ethanol Blended Fuel Spray Characteristics on the Reduction of Exhaust Emissions in a Common-Rail Diesel Engine," *ASME J. Energy Resour. Technol.*, **132**(4), p. 042201.
- Xing-Cai, L., Jian-Guang, Y., Wu-Gao, Z., and Zhen, H., 2004, "Effect of Cetane Number Improver on Heat Release Rate and Emissions of High-Speed Diesel Engine Fueled With Ethanol-Diesel Blend Fuel," *Fuel*, **83**(14–15), pp. 2013–2020.
- Sharma, N., Agarwal, R. A., and Agarwal, A. K., 2019, "Particulate Bound Trace Metals and Soot Morphology of Gasohol Fueled Gasoline Direct Injection Engine," *ASME J. Energy Resour. Technol.*, **141**(2), p. 022201.
- Knothe, G., Matheaus, A. C., and Ryan T. W., III, 2003, "Cetane Numbers of Branched and Straight Chain Fatty Esters Determined in an Ignition Quality Tester," *Fuel*, **82**(8), pp. 971–975.
- Thomas, G., Feng, B., Veeraragavan, A., Cleary, M. J., and Drinnan, N., 2014, "Emissions From DME Combustion in Diesel Engines and Their Implications on Meeting Future Emission Norms: A Review," *Fuel Process. Technol.*, **119**, pp. 286–304.
- Singh, A. P., and Agarwal, A. K., 2017, "CI/PCCI Combustion Mode Switching of Diesohol Fueled Production Engine," SAE Technical Paper No. 2017-01-0738.
- Satsangi, D. P., and Tiwari, N., 2018, "Experimental Investigation on Combustion, Noise, Vibrations, Performance and Emissions Characteristics of Diesel/n-Butanol Blends Driven Genset Engine," *Fuel*, **221**, pp. 44–60.
- Singh, A. P., and Agarwal, A. K., 2016, "Effect of Intake Charge Temperature and EGR on Biodiesel Fueled HCCI Engine," SAE Technical Paper No. 2016-28-0257.
- Song, J., Zello, V., Boehman, A. L., and Waller, F. J., 2004, "Comparison of the Impact of Intake Oxygen Enrichment and Oxygenation on Diesel Combustion and Emissions," *Energy Fuels*, **18**(5), pp. 1282–1290.
- Choi, C. Y., and Reitz, R. D., 1999, "An Experimental Study on the Effects of Oxygenated Fuel Blends and Multiple Injection Strategies on DI Diesel Engine Emissions," *Fuel*, **78**(11), pp. 1303–1317.
- Manin, J., Skeen, S., Pickett, L., Kurtz, E., and Anderson, J., 2014, "Effects of Oxygenated Fuels on Combustion and Soot Formation/Oxidation Processes," *SAE Int. J. Fuels Lubr.*, **7**(3), pp. 704–717.
- Cheng, A. S., Dibble, R. W., and Buchholz, B. A., 2002, "The Effect of Oxygenates on Diesel Engine Particulate Matter," SAE Technical Paper No. 2002-01-1705.
- Xingcai, L., Zhen, H., Wugao, Z., and Degang, L., 2004, "The Influence of Ethanol Additives on the Performance and Combustion Characteristics of Diesel Engines," *Combust. Sci. Technol.*, **176**(8), pp. 1309–1329.
- Singh, A. P., and Agarwal, A. K., 2018, "Low Temperature Combustion Engines and Mode Switching Strategies: A Review," *J. Energy Environ. Sustainability*, **6**, pp. 40–45.
- Campos-Fernández, J., Arnal, J. M., Gómez, J., and Dorado, P., 2012, "A Comparison of Performance of Higher Alcohols/Diesel Fuel Blends in a Diesel Engine," *Appl. Energy*, **95**, pp. 267–275.
- Eugene, E. E., Bechtold, R. L., Timbario, T. J., and McCallum, P. W., 1984, "State-of-the-Art Report on the Use of Alcohols in Diesel Engines," SAE Technical Paper No. 840118.
- Broukhiyan, E. M. H., and Lestz, S. S., 1981, "Ethanol Fumigation of a Light Duty Automotive Diesel Engine," SAE Technical Paper No. 811209.
- Hansen, A. C., Zhang, Q., and Lyne, P. W. L., 2005, "Ethanol Diesel Fuel Blends—A Review," *Bioresour. Technol.*, **96**(3), pp. 277–285.
- Marek, N., and Evanoff, J., 2001, "The Use of Ethanol Blended Diesel Fuel in Unmodified, Compression Ignition Engines: an Interim Case Study," Proceedings of the Air and Waste Management Association 94th Annual Conference and Exhibition, Orlando, FL, June 24–28.
- Hansen, A. C., Hornbacker, R. H., Zhang, Q., and Lyne, P. W. L., 2001, "On Farm Evaluation of Diesel Fuel Oxygenated With Ethanol," *ASAE Annual International Meeting*, Sacramento Convention Center, Sacramento, CA, July 30–Aug. 1.
- Singh, A. P., and Agarwal, A. K., 2016, "Diesohol, Diesohol, and Diesohol Fueled HCCI Engine Development," *ASME J. Energy Resour. Technol.*, **138**(5), p. 052212.
- Kwancharoen, P., Luengnarumitchai, A., and Jai-In, S., 2007, "Solubility of a Diesel-Biodiesel-Ethanol Blend, its Fuel Properties, and its Emission Characteristics From Diesel Engine," *Fuel*, **86**(7–8), pp. 1053–1061.
- Smerkowska, B., 2011, "Biobutanol—Production and Application in Diesel Engines," *Chemik*, **65**(6), pp. 549–556.
- Rakopoulos, D. C., Rakopoulos, C. D., Giakoumis, E. G., Dimaratos, A. M., and Kyritsis, D. C., 2010, "Effects of Butanol-Diesel Fuel Blends on the Performance and Emissions of a High-Speed DI Diesel Engine," *Energy Convers. Manage.*, **51**(10), pp. 1989–1997.
- Chao, M. R., Lin, T. C., Chao, H. R., Chang, F. H., and Chen, C. B., 2001, "Effects of Methanol-Containing Additive on Emission Characteristics From a Heavy-Duty Diesel Engine," *Sci. Total Environ.*, **279**(1–3), pp. 167–179.
- Huang, Z. H., Lu, H. B., Jiang, D. M., Zeng, K., Liu, B., Zhang, J. Q., and Wang, X. B., 2004, "Combustion Characteristics and Heat Release Analysis of a Compression Ignition Engine Operating on a Diesel/Methanol Blend," *IMEchE*, **218**(9), pp. 1011–1024.
- Wang, W. G., Clark, N. N., Lyons, D. W., Yang, R. M., Gautam, M., Bata, R. M., and Loth, J. L., 1997, "Emissions Comparisons From Alternative Fuel Buses and Diesel Buses With a Chassis Dynamometer Testing Facility," *Environ. Sci. Technol.*, **31**(11), pp. 3132–3137.
- Guo, Z., Li, T., Dong, J., Chen, R., Xue, P., and Wei, X., 2011, "Combustion and Emission Characteristics of Blends of Diesel Fuel and Methanol-to-Diesel," *Fuel*, **90**(3), pp. 1305–1308.
- Shore, P. R., Humphries, D. T., and Hadded, O., 1993, "Speciated Hydrocarbon Emissions from Aromatic, Olefinic and Paraffinic Model Fuels," SAE Technical Paper No. 930373.
- Park, W., Park, S., Reitz, R. D., and Kurtz, W., 2017, "The Effect of Oxygenated Fuel Properties on Diesel Spray Combustion and Soot Formation," *Combust. Flame*, **180**, pp. 276–283.
- Canakci, M., Sayin, C., Ozsezen, A. N., and Turkcan, A., 2009, "Effect of Injection Pressure on the Combustion, Performance, and Emission Characteristics of a Diesel Engine Fueled With Methanol-Blended Diesel Fuel," *Energy Fuels*, **23**(6), pp. 2908–2920.
- Singh, A. P., and Agarwal, A. K., 2018, "Evaluation of Fuel Injection Strategies for Biodiesel-Fueled CRDI Engine Development and Particulate Studies," *ASME J. Energy Resour. Technol.*, **140**(10), p. 102201.
- Sayin, C., Ilhan, M., Canakci, M., and Gumus, M., 2009, "Effect of Injection Timing on the Exhaust Emissions of a Diesel Engine Using Diesel-Methanol Blends," *Renewable Energy*, **34**(5), pp. 1261–1269.
- Murayama, T., Miyamoto, N., Yamada, T., Kawashima, J. I., and Itow, K., 1982, "A Method to Improve the Solubility and Combustion Characteristics of Alcohol-Diesel Fuel Blends," SAE Technical Paper No. 821113.
- Bayraktar, H., 2008, "An Experimental Study on the Performance Parameters of an Experimental CI Engine Fueled With Diesel-Methanol-Dodecanol Blends," *Fuel*, **87**(2), pp. 158–164.
- Agarwal, A. K., Srivastava, D. K., Dhar, A., Maurya, R. K., Shukla, P. C., and Singh, A. P., 2013, "Effect of Fuel Injection Timing and Pressure on Combustion, Emissions and Performance Characteristics of a Single Cylinder Diesel," *Fuel*, **111**, pp. 374–383.
- Agarwal, A. K., Singh, A. P., and Pal, A., 2017, "Effect of Laser Parameters and Compression Ratio on Particulate Emissions From a Laser Ignited Hydrogen Engine," *Int. J. Hydrogen Energy*, **42**(15), pp. 10622–10635.
- Indian Standard IS: 14273, 1999, *Automotive Vehicles—Exhaust Emissions—Gaseous Pollutants From Vehicles Fitted With Compression Ignition Engines—Method of Measurement*, Bureau of Indian Standards, New Delhi, India.
- Maurya, R. K., and Agarwal, A. K., 2015, "Experimental Investigations of Particulate Size and Number Distribution in an Ethanol and Methanol Fueled HCCI Engine," *ASME J. Energy Resour. Technol.*, **137**(1), p. 012201.
- TSI, 2009, *Engine Exhaust Particle Sizer™ Spectrometer Model 3090. Operation and Service Manual*, TSI Inc., Shoreview, MN.
- Agarwal, A. K., Dhar, A., Srivastava, D. K., Maurya, R. K., and Singh, A. P., 2013, "Effect of Fuel Injection Pressure on Diesel Particulate Size and Number Distribution in a CRDI Single Cylinder Research Engine," *Fuel*, **107**, pp. 84–89.
- Baldauf, R. W., Devlin, R. B., Gehr, P., Giannelli, R., Hassett-Sipple, B., Jung, H., Martini, G., McDonald, J., Sacks, J. D., and Walker, K., 2016, "Ultrafine Particle Metrics and Research Considerations: Review of the 2015 UFP Workshop," *Int. J. Environ. Res. Public Health*, **13**(11), p. 1054.
- Singh, A. P., Pal, A., and Agarwal, A. K., 2016, "Comparative Particulate Characteristics of Hydrogen, CNG, HCNG, Gasoline and Diesel Fueled Engines," *Fuel*, **185**(1), pp. 491–499.
- Shukla, P. C., Gupta, T., Gupta, N., and Agarwal, A. K., 2017, "A Qualitative Correlation Between Engine Exhaust Particulate Number and Mass Emissions," *Fuel*, **202**, pp. 241–245.